Chinese Chemical Letters 34 (2023) 108569

Contents lists available at ScienceDirect

Chinese Chemical Letters

journal homepage: www.elsevier.com/locate/cclet

Oxygen doping modulating thermal-activated charge transport of reduced graphene oxide for high performance temperature sensors

Liqian Yuan[a], Zhongwu Wang[a], Yancheng Meng[d], Shuguang Wang[a,*], Yajing Sun[a,*], Yinan Huang[a,b,*], Liqiang Li[a,b,c,*], Wenping Hu[a,b,c]

[a] Tianjin Key Laboratory of Molecular Optoelectronic Sciences, Department of Chemistry, Institute of Molecular Aggregation Science, Tianjin University, Tianjin 300072, China
[b] Joint School of National University of Singapore and Tianjin University, International Campus of Tianjin University, Binhai New City, Fuzhou 350207, China
[c] Haihe Laboratory of Sustainable Chemical Transformations, Tianjin 300192, China
[d] Key Laboratory for Intelligent Nano Materials and Devices of the Ministry of Education, State Key Laboratory of Mechanics and Control of Mechanical Structures, Institute for Frontier Science, Nanjing University of Aeronautics and Astronautics, Nanjing 210016, China

ARTICLE INFO

Article history:
Received 6 March 2023
Revised 9 May 2023
Accepted 11 May 2023
Available online 12 May 2023

Keywords:
Temperature sensors
Reduced graphene oxide (RGO)
Oxygen doping
Temperature dependence of thermal-activated charge transport
Sensitivity
Response time

ABSTRACT

Graphene and its derivatives have sparked intense research interest in wearable temperature sensing due to their excellent electric properties, mechanical flexibility, and good biocompatibility. Despite these advantages, the weak temperature dependence of charge transport makes them difficult to achieve a highly sensitive temperature response, which is one of the remaining bottlenecks in the progress towards practical applications. Unfortunately, detailed knowledge about the key factors of the charge transport temperature dependence in this material that determines the critical performance of electrical sensors is very limited up to now. Here, we reveal that oxygen absorption on the ultrathin reduced graphene oxide (RGO) films (~3 nm) can significantly increase their conductance activation energy over 200% and thus greatly improve the temperature dependence of thermal-activated charge transport. Further investigations suggest that oxygen introduces the deep acceptor states, distributed at an energy level ~0.175 eV from the valence-band maximum, which allows a highly temperature-dependent impurity ionization process and the resulting vast holes release in a wide temperature range. Remarkably, our temperature sensors based on oxygen-doped ultrathin RGO films show a high sensitivity with temperature conductive coefficient of 14.58% K^{-1}, which is one order of magnitude higher than the reported CNT or graphene-based devices. Moreover, the ultrathin thickness and high thermal conductivity of RGO film allow an ultrafast response time of ~86 ms, which represents the best level of temperature sensors based on soft materials. Profiting from these advantages, our sensors show good capacity to identify the slight temperature difference of human body, monitor respiratory rate, and detect the environmental temperature. This work not only represents substantial performance advances in temperature sensing, but also provides a new approach to modulate the charge transport temperature dependence, which could be benefited to both device design and fundamental research.

Temperature sensors are widely used in numerous conventional fields of human society and serve as one of key components of some emerging applications such as wearable electronics, e-skins and human health monitoring [1–5]. The common temperature sensors, based on metals, ceramics or silicon, are limited by either poor performance (*e.g.*, low sensitivity and slow response) or rigid, bulk structure and are not compatible with flexible electronics [4,6,7]. Reduced graphene oxide (RGO), as a derivative of graphene, has the advantage of large-scale and low-cost solution processability with the excellent properties inherited from graphene, such as atomic thickness, high thermal conductivity and mechanical flexibility [8–12]. With these advantages, RGO is believed as a promising candidate for the new generation temperature sensors entering the market of flexible electronics, and many prototype devices have

* Corresponding authors.
E-mail addresses: wsg123@tju.edu.cn (S. Wang), syj19@tju.edu.cn (Y. Sun), huangyn@tju.edu.cn (Y. Huang), lilq@tju.edu.cn (L. Li).

https://doi.org/10.1016/j.cclet.2023.108569
1001-8417/

been demonstrated. However, the weak temperature dependence of charge transport in RGO makes the sensing performance highly limited. The pressing bottleneck in the progress of RGO sensors towards practical applications is the lack of understanding of the factors that govern their temperature dependence of charge transport.

It is reported that RGO undergoes a transformation from semiconductor to semimetal as sp^3 hybridized carbon atoms are gradually reduced to the extended sp^2 conjugated network in the reduction process, significantly decreasing the localized tail states resulting from structure disorder [13]. It makes the charge transport gradually transform from thermal-activated hopping to band-like and thus decreases temperature dependence of charge transport. It seems a feasible method to improve the temperature dependence of charge transport by increasing the ratio of sp^3 hybridized carbon atoms in RGO through controllable reduction process [14]. However, it would critically scarify the key properties of RGO, such as electrical and thermal conductivities, which leads to a performance tradeoff between sensitivity and other important parameters. Up to now, how to safely improve the charge transport temperature dependence of RGO is still a great challenge.

Here, we develop a strategy to overcome this challenge by minimizing the thickness of RGO films (~3 nm) to increase oxygen absorption, which significantly increases the conductance activation energy of RGO and thus greatly improves the temperature dependence of thermal-activated charge transport. Remarkably, our RGO sensors show high sensitivity with temperature conductive coefficient of 14.58% K^{-1}, which is one order of magnitude higher than the reported CNT or graphene-based devices. Moreover, the ultrathin thickness and high thermal conductivity of RGO film allow an ultrafast response time ~86 ms, which represents the best level of temperature sensors based on soft materials.

The device structure schematic diagram is shown in Fig. 1a. To obtain a continuous, uniform and ultrathin graphene oxide (GO) film, (3-aminopropyl)triethoxysilane (APTES) with two functional groups was used to modify the polyimide (PI) surface, and then GO sheets were assembled onto APTES through covalent bonds [15–17]. Through these two processes, the ultrathin (about 3 nm) GO film (Figs. 1b and c) was formed with the large area continuation and uniformity (Fig. S1 in Supporting information). Notably, the covalently-bonded GO film showed excellent resistance toward solvent ultrasonic treatment and mechanical scratch possesses (Movie S1 in Supporting information), indicating its high mechanical robustness. The device was accomplished after Au electrode patterning by thermal deposition combined with a shadow mask and RGO film thermal reduction to form the GO film (for details, see Supporting information). All fabrication processes were low-cost and applicable to large area, which would be very meaningful for some applications such as wearable electronics.

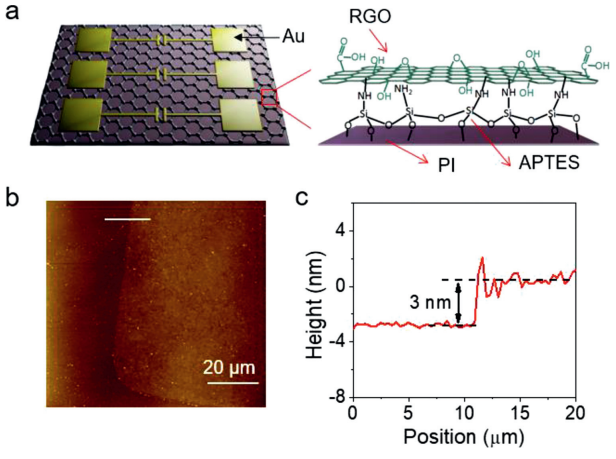

Fig. 1. Structure of the ultrathin RGO sensors. (a) Schematic of the ultrathin RGO temperature sensors and chemical structure of ultrathin RGO film. (b) AFM image and (c) section profile of the edge of an ultrathin GO film.

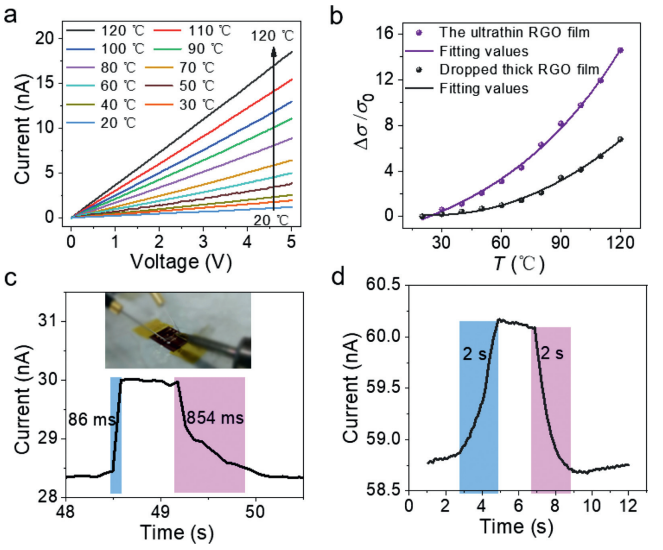

Fig. 2. Response time and sensitivity of the ultrathin RGO sensor. (a) *I-V* curves of ultrathin RGO sensor in the temperature range of 20–120 °C (temperature step set as 10 °C). (b) Conductivity variation of the ultrathin and the thick RGO sensors with temperature. Response time of (c) the ultrathin RGO sensor (~3 nm) and (d) the thicker RGO sensor (~200 nm).

To investigate the sensing property of the ultrathin RGO sensor, the sensor was placed on a thermal platform and temperature was tuned between 20 °C to 120 °C. Figs. 2a and b and Fig. S2 (Supporting information) show the *I-V* curves and the conductivity variation with temperature, respectively. The conductivity of ultrathin RGO sensor raised by near one and a half orders of magnitude when temperature was increased from 20 °C to 120 °C and sensitivity ($((\Delta\sigma/\sigma_0)/dT \times 100\%)$) was about 14.58% K^{-1}. However, over the same temperature range, the conductivity of 30 nm, 80 nm and 200 nm-thickness sensors changes by 12, 10 and 6.5 times, respectively, which is significantly lower than that of the ultra-thin sensors (Figs. S3 and S4 in Supporting information). A linear relationship between $\ln(\sigma)$ and $1000/T$ (Fig. S5 in Supporting information) shows a good fit with Arrhenius equation, which implies that the carrier transport mechanism in ultrathin RGO film is based on hopping model [18,19]. Such high sensitivity of our device exceeds most of reported temperature sensors, especially greatly higher than CNT [4] and graphene-based devices [20]. To test the response speed of the ultrathin RGO sensor, a thermal source (electric iron covered with PI tape) was quickly in touch with and then removed far from the sensor. Deserve to be mentioned, the bare ultrathin RGO film without any package is so robust that can withstand touch, which benefits from the covalent assembly as demonstrated in Movie S1. As expected, our device showed a quite impressive high-speed response time of 86 ms and a recovery time of about 854 ms (Fig. 2c, Fig. S6 and Movie S2 in Supporting information), which is superior to the reported temperature sensors with thick RGO active layers [10,21–25]. The key performance, materials and type of some recently reported temperature sensors are summarized in Table 1 [1,4,10,25–29]. By the way, the initial conductivity of the ultrathin RGO films depends on their reduction level, but it has insignificant influence on their temperature sensing performance (Figs. S7 and S8 in Supporting information). As designed, in our sensor based on the ultrathin RGO film remarkably decreases the thermal conduction time, and therefore significantly improves the response speed. For comparison, the thicker RGO film (about 200 nm) prepared by the drop-casting method showed a longer re-

Table 1
Comparison between various temperature sensors.

Materials	Device type	Response/Recovery time *	Sensitivity (TCC #)	Temperature change (°C)	Temperature resolution (°C)	Ref.
Plastic Ag_2S	Thermoelectricity	0.11 s/0.11 s	4.9% K^{-1} #	24–34	0.05	[1]
SWCNTs	Transistor	1.8 s/3 s	1% K^{-1} #	15–45	–	[4]
RGO fiber	Thermistor	7 s/20 s	0.19% K^{-1} #	30–80	3	[10]
Graphite/polymer	Thermistor	100 ms/-	−0.19% K^{-1} #	25–50	0.1	[25]
CSNF-Pt	Thermistor	13.12 s/-	1.78% K^{-1} #	35–63	3.5	[26]
PENB:F4TCNQ	Thermistor	9.2 s/-	1.9% K^{-1} #	20–60	2	[27]
PEDOT/TPU	Thermistor	27 s/30 s*	0.96% K^{-1} #	20–40	0.2	[28]
RGO/PU	Transistor	10 s*/-	1.36% K^{-1} #	30–80	0.2	[29]
Ultrathin RGO	Thermistor/Transistor	86 ms/0.85 s	14.58% K^{-1}	20–120	0.2	This work

* Some response time and # the temperature coefficient of conductivity (TCC) are estimated based on the figure in the literatures. TCC is defined as $TCC = (\Delta\sigma/\sigma_0)/dT \times 100\%$, which is the key parameter to assess the sensitivity of the sensor.

sponse and recovery time of about 2 s (Fig. 2d). The difference in response speed of the RGO sensors based on ultrathin film and thick film is expected, but it is surprising that the thermal response of the ultrathin RGO film is much higher than that of the thick film, with corresponding activation energy E_a^{ultra} of 0.29 eV and E_a^{thick} of 0.135 eV extracted from Fig. S5 by Arrhenius equation (Eq. 1):

$$\sigma = \sigma_0 exp\left(-E_a/k_BT\right) \quad (1)$$

where σ and σ_0 are the conductivity at temperature T and absolute zero, respectively, and k_B is Boltzmann constant. And the striking discrepancy in activation energy suggests that some latent factors significantly alter the charge transport temperature dependence of RGO.

It is well known that aromatic molecules, 2D carbon material could adsorb the oxygen and form p-type doping [30–33]. We speculate oxygen doping may have an underlying impact on the charge transport of RGO and the higher concentration of adsorbed oxygen in ultrathin RGO allows higher thermal response (submicrometer-thick GO membranes can be completely impermeable to any gas [34]). To testify the effect of doped oxygen on temperature response, the ultrathin and the thick RGO sensors were measured in a high vacuum (~10^{-4} Pa) to remove the adsorbed oxygen. The temperature was raised from 20 °C to 70 °C. It can be seen from Fig. 3a that the current of the ultrathin RGO shows a slight increase in vacuum. Remarkably, when a small amount of O_2 was introduced into vacuum chamber to a pressure of about 10^{-1} Pa, the current immediately increased significantly. In contrast, the current change of the thick RGO is obviously less than that of the ultrathin RGO. These results clearly indicate adsorbed oxygen have an important impact on the temperature dependence of charge transport in RGO and also demonstrate the key role of ultrathin film in high thermal response.

To further verify the doping effect by oxygen absorption, we used electron paramagnetic resonance spectroscopy (EPR) to track unpaired electrons of RGO in air (Supporting information). As shown in Fig. 3b, the RGO film in the static magnetic field exhibits an identifiable EPR signal with $g = 2.0017$ and peak-to-peak linewidth (ΔH_{pp}) ≈ 3.4 G, which is assigned to the RGO cation radical [35]. After confirming the existence of RGO cation radical, its putative partner should be superoxide anion (O_2^-), but its EPR signal is usually too broad to be directly observed because of fast spin relaxation. To confirm the O_2^- existing, a spin trapping agent 5,5-dimethyl-1-pyrroline N-oxide (DMPO) was used. After the RGO film was immersed in trapping agent diluent for 30 min, the characteristic EPR signal of the adduct DMPO-•OOH of DMPO with the superoxide anion (O_2^-) was observed, with six peaks of equal height and hyperfine coupling constants A_N ≈ 13 G and $A_{h\beta}$ ≈ 8 G. These EPR signals are direct indicators of the existence of the geminate RGO cation radical and O_2^-, revealing that an acceptor doping readily occurs on RGO by spontaneous oxygen absorption in air.

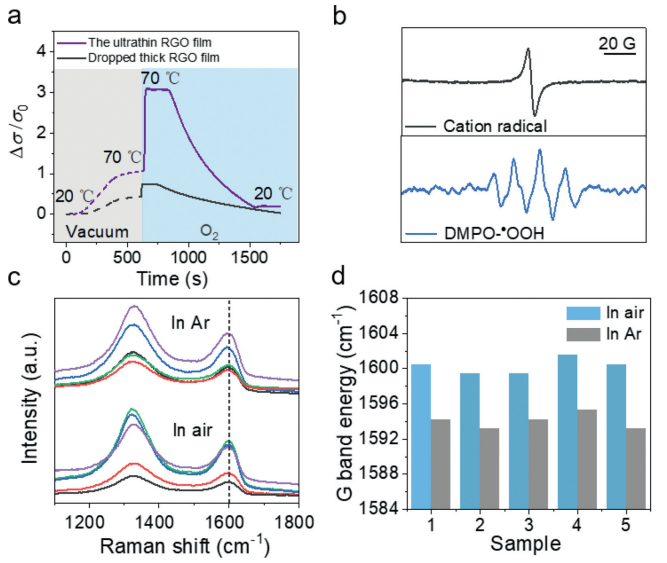

Fig. 3. Effect of oxygen doping on high sensitivity of the ultrathin RGO sensor. (a) The current of RGO sensor measured in vacuum when temperature changes from 20 °C to 70 °C. (b) The EPR signals of cation radical and O_2^- (DMPO-•OOH) in RGO. DMPO-•OOH shows the six peaks with the hyperfine coupling constants A_N ≈ 15 G and $A_{h\beta}$ ≈ 11 G. (c, d) Raman spectrum and statistics of the Raman G band frequency of five ultrathin RGO films in air and Ar.

This point was further confirmed by Raman measurements. The Raman G band of graphene upshift is widely interpreted as a measure of carrier doping [30,32,33,36]. Therefore, the G band frequency, ωG, of ultrathin RGO film was measured both before (referred as untreated sample) and after annealing and encapsulation in an Ar atmosphere (referred as treated sample, for details, see Supporting information). The ωG of the untreated samples upshifts obviously compared to those treated samples (Figs. 3c and d). The ωG of ultrathin RGO films is observed to be 1600 cm^{-1} in air and 1594 cm^{-1} in Ar, where their standard deviation is 1 cm^{-1}. This result suggests that O_2 in the air was adsorbed, thus forming reversible doping on ultrathin RGO film.

To investigate the mechanism that oxygen doping modulates the temperature dependence of charge transport in RGO, the ultrathin RGO field-effect transistors (FETs) were prepared (Supporting information) and their temperature response was investigated over temperature range of 20–70 °C. The transfer curves of the RGO FET were measured in air and vacuum, respectively (Figs. 4a and b), and the FETs show typical p-type behaviors in air but n-type behaviors in vacuum, which is contributed to the compensation of existing electrons by oxygen doping in air. The change of the minimum drain current ($I_{ds,\,min}$) *versus* temperature in air and vacuum is shown in Fig. S9a (Supporting information). The plot of ln($I_{ds,\,min}$) as a function of 1000/T (Fig. S9b in Support-

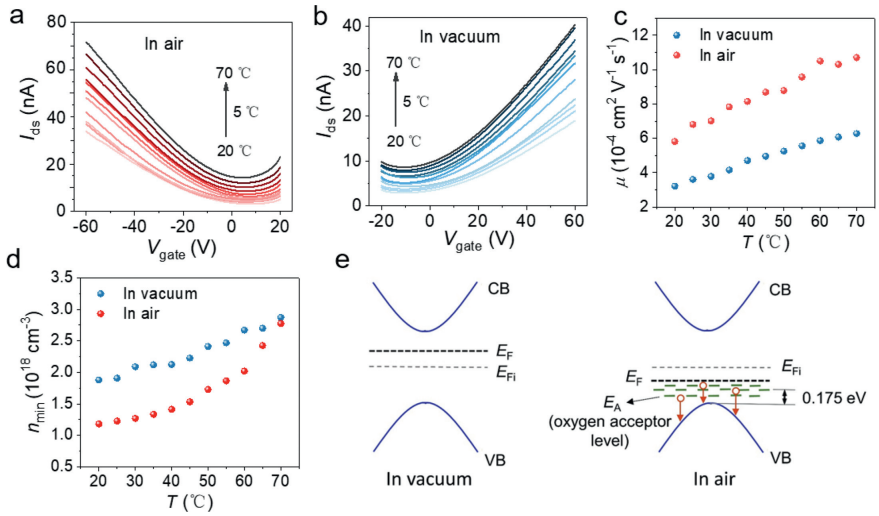

Fig. 4. Characteristics of ultrathin RGO FET in air and vacuum. (a, b) Transfer characteristics of ultrathin RGO FET measured over the temperature range of 20–70 °C in air and vacuum. V_{ds}= 5 V. (c) The carrier mobility of ultrathin RGO FET at variable temperature in air and vacuum. (d) The carrier concentration at variable temperature in air and vacuum. (e) Band diagrams of RGO before and after oxygen doping. E_F, E_{Fi}, CB and VB represent the Fermi level, the intrinsic Fermi level, the conduction band and the valence band, respectively.

ing information) shows a good fit with the Arrhenius model in both air and vacuum, from which the conductive activation energy (E_a) of ultrathin RGO film can be calculated by the slope to be 0.16 eV in vacuum and 0.23 eV in air, respectively. To further investigate the origin of activation energy change, we extracted the temperature-dependent mobilities in linear region (μ) of the ultrathin RGO FETs in vacuum and air by field-effect method, $I_{ds} = C_i \mu V_{ds}(W/L)(V_{gs} - V_t)$, where W and L are the width and length of the conducting channel, C_i is the unit-area capacitance of the dielectric layer. As shown in Fig. 4c, the temperature dependence of mobilities in the two FETs is almost identical with the same hopping activation energy of ~0.086 eV (Fig. S10 in Supporting information), which indicates that oxygen doping does not alter the density of localized states related to hopping. Then, off-state carrier density (n) of the ultrathin RGO FETs in vacuum and air is calculated by $\sigma = ne\mu$ using the minimum current of transfer curves. In both cases, the carrier density increases obviously with increasing temperature, but its temperature dependence is more pronounced in air in Fig. 4d, which suggests the increase of conductive activation energy by oxygen doping is mainly due to the contribution of carrier density. We speculate that the temperature dependence improvement in air may be derived from the deep acceptor states introduced by oxygen doping [37]. The deep acceptor states result in a temperature-dependent impurity ionization process in a wide temperature range, in which vast holes are released into the valence band, leading to significantly increased conductivity (Fig. 4e). The energetic level of oxygen acceptor states, *i.e.*, can be roughly estimated to be 0.175 eV (Fig. S11 in Supporting information) from the valence-band maximum by Eq. 2 [38]:

$$n \approx \sqrt{\frac{N_A N_V}{2}} exp\left(-\frac{E_A - E_V}{2k_B T}\right) \quad (2)$$

where N_A and N_V are density of oxygen acceptors and valence band, respectively, and E_A and E_V are energy level of oxygen acceptors and valence-band edge, respectively. The thickness-dependent temperature sensitivity of RGO film can also be explained. When the thickness of the RGO film is reduced, the absorbed oxygen concentration increases, resulting in more impurities ionization with the increase of temperature. Therefore, the thinner RGO film has a relatively high temperature sensitivity.

Benefiting from high sensitivity and fast response of ultrathin RGO, the sensors can monitor a small temperature change of 0.2 °C over a range of 37–38 °C as shown in Fig. 5a. This resolution is better than, at least comparable to, the reported values (Table 1). In fact, high sensitivity suggests that our sensor may hold promise for higher resolution. However, due to the limitation of our experiment setup, we could not obtain smaller temperature change in a continuous and reliable mode. In addition, this temperature range fits with human body, indicating the potential of our sensor in the wearable electronics. A step-like current curve with temperature range of 20–50 °C is shown in Fig. S12 (Supporting information), which presents that the RGO device works stably at different temperature. To compare the sensing performance of the ultrathin RGO sensor with the widely-used thermocouple, our device next to a commercial thermocouple was heated and cooled continuously over temperature range of 20–80 °C. The temperature spectra measured from our device and thermocouple is shown in Fig. 5b. Extraordinarily, these two sensors show the almost identical trend, indicating the accuracy, reliability, and high response speed of the ultrathin RGO sensor that can be comparable to the commercial temperature sensor.

To demonstrate the possibility of the ultrathin RGO sensor for detecting the temperature of human body, the response of the device covered with PI tape was investigated when touched with finger pulp, finger dorsum and a plastic tube, respectively. As shown in Fig. 5c, the device responded quickly and can distinguish the small temperature difference of about 0.4 °C between finger pulp and finger dorsum that is measured with an infrared thermometer. The pressure exerted by the plastic tube caused only a weak signal disturbance. The whole experiment was shown in Movie S3 (Supporting information). These comparative results demonstrate that our sensor has high temperature resolution and may distinguish the human body with small different temperature, and that our sensor shows good immunity to the pressure which is important for the practical application in the complicated environment. Fig. 5d shows that the device encapsulated with scotch tape monitors respiratory rate by measuring the heat of breathing gas. It is only about 3 s for a normal breath, which proposes a high requirement on the response time of the device. Our sensor can well capture the respiratory state of human, which benefits from the fast response speed and high sensitivity. To demonstrate the flexibility of the ultrathin RGO sensor, the temperature response of the sensor

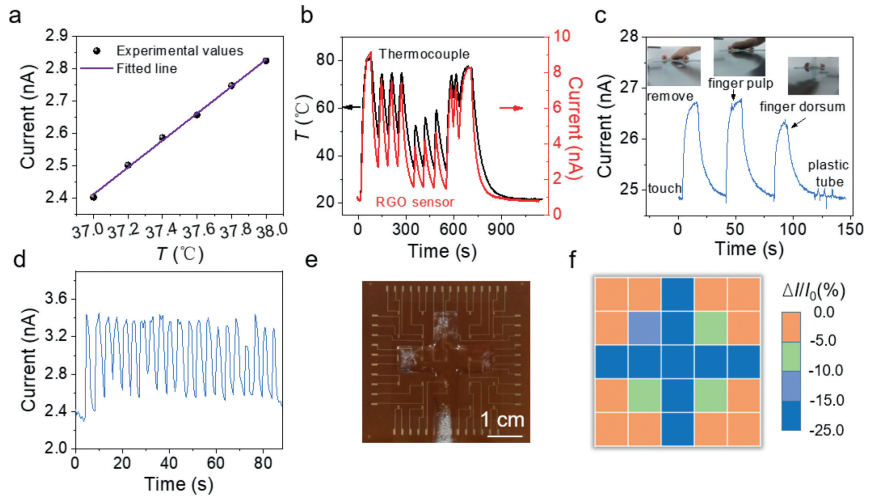

Fig. 5. Accurate measurement and exemplary applications of the ultrathin RGO sensor. (a) Resolution of the temperature sensor. (b) The temperature measurement of ultrathin RGO sensor and thermocouple. (c) The current response of the ultrathin RGO sensor to finger touch. (d) The device monitored respiratory rate by measuring the heat of breathing gas. (e) Photograph of a 5×5 ultrathin RGO sensor array. (f) Temperature distribution measured from the sensor array.

after different bending times and under bending radius was measured, respectively. Fig. S13a (Supporting information) shows that the temperature response curve did not change significantly during the process of sensor bending from 0 to 4000 times. In addition, the sensor shows the same temperature response characteristics as when placed horizontally at a tensile radius of 3.5, 6 and 8 mm (Fig. S13b in Supporting information). These tests indicate the potential of the ultrathin RGO sensors in wearable electronics and human health monitoring. To detect the environment thermal irradiation, the device was irradiated with infrared light at different distances (Fig. S14 and Movie S4 in Supporting information). The output sensing signal well matches the distance (*i.e.*, the temperature), indicating the potential of our sensor for monitoring the environmental temperature. For practical application, sensor arrays are generally required. To prove this point, a 5×5 ultrathin RGO sensor array was fabricated and encapsulated with scotch tape for conducting temperature mapping. The normalized currents ($\Delta I/I_0 \times 100\%$) of the array were measured when a cross-shaped ice cube was placed on it (Fig. 5e). The mapping of the temperature distribution *via* the measurement of the normalized drain current is shown in Fig. 5f. This experiment exhibits precise temperature sensing capability of the ultrathin RGO sensor array and reveals its potential for the application in multipoint measurements.

In conclusion, we demonstrate an effective strategy based on spontaneous oxygen absorption to significantly improve the temperature dependence of thermal-activated charge transport in RGO. The mechanism behind excellent performance is unraveled that oxygen introduce the deep acceptor states, distributed at an energy level ~0.175 eV from the valence-band maximum, which allows a highly temperature-dependent impurity ionization process and the resulting vast holes release in a wide temperature range. This effect is dramatically enhanced by minimizing the thickness of RGO films. Remarkably, our temperature sensors based on oxygen-doped ultrathin RGO films exhibit a high sensitivity of 14.58% K^{-1} and a high-speed response time of 86 ms. The high sensitivity and good reliability make temperature resolution of our device as small as 0.2 °C. This sensor can detect human touch, monitor respiratory rate, distinguish the environmental thermal irradiation, and achieve multipoint measurements. The high sensing performance, easy fabrication and low-cost enable the ultrathin RGO sensor to be highly promising for emerging applications such as wearable devices and human-machine interaction applications.

Declaration of competing interest

The authors declare that they have no known competing financial interests or personal relationships that could have appeared to influence the work reported in this paper.

Acknowledgments

The authors are grateful to National Key Research and Development Program (Nos. 2018YFA0703200, 2016YFB0401100), National Natural Science Foundation of China (Nos. 52225304, 52073210, 52203236, 52121002), Natural Science Foundation of Tianjin City (Nos. 19JCZDJC37400, 19JCJQJC62600), and Haihe Laboratory of Sustainable Chemical Transformations.

Supplementary materials

Supplementary material associated with this article can be found, in the online version, at doi:10.1016/j.cclet.2023.108569.

References

[1] X.F. Zhao, S.Q. Yang, X.H. Wen, et al., Adv. Mater. 34 (2022) 2107479.
[2] J. Shin, B. Jeong, J. Kim, et al., Adv. Mater. 32 (2020) 1905527.
[3] J. Shin, B. Jeong, J. Kim, et al., Adv. Mater. 32 (2020) 2070014.
[4] S.Y. Hong, Y.H. Lee, H. Park, et al., Adv. Mater. 28 (2016) 930–935.
[5] Q. Ding, Z. Zhou, H. Wang, et al., SmartMat 4 (2023) e1141.
[6] Y. Lv, M. Hu, M. Wu, Z. Liu, Surf. Coat. Technol. 201 (2007) 4969–4972.
[7] Z. Wu, C. Li, J. Hartings, et al., J. Micromech. Microeng. 27 (2016) 025001.
[8] J. Zhao, Y. Zhang, Y. Huang, et al., J. Mater. Chem. A 7 (2019) 972–978.
[9] E.A. Araya-Hermosilla, M. Carlotti, F. Picchioni, et al., Polymers 12 (2020) 923 (Basel).
[10] T.Q. Trung, H.S. Le, T.M.L. Dang, et al., Adv. Healthc. Mater. 7 (2018) e1800074.
[11] H. Chen, J. Huang, J. Liu, et al., J. Mater. Chem. A 9 (2021) 23243–23255.
[12] Z. Tian, P. Song, Z. Yang, Q. Wang, Chin. Chem. Lett. 31 (2020) 2067–2070.
[13] T. Yokota, Y. Inoue, Y. Terakawa, et al., Proc. Natl. Acad. Sci. U. S. A. 112 (2015) 14533–14538.
[14] Z. Yang, T. Huang, P. Cao, et al., ACS Appl. Mater. Interfaces 14 (2022) 18110–18119.
[15] F. Li, H. Xue, X. Lin, et al., ACS Appl. Mater. Interfaces 14 (2022) 43844–43852.
[16] T.Q. Trung, S. Ramasundaram, B.U. Hwang, N.E. Lee, Adv. Mater. 28 (2016) 502–509.
[17] G. Eda, C. Mattevi, H. Yamaguchi, et al., J. Phys. Chem. C 113 (2009) 15768–15771.
[18] T.Q. Trung, T.M.L. Dang, S. Ramasundaram, et al., ACS Appl. Mater. Interfaces 11 (2018) 2317–2327.
[19] J. Chen, F. Chi, L. Huang, et al., Carbon 110 (2016) 34–40.
[20] X. Chen, S. Zhang, K. Wu, et al., Adv. Electron. Mater. 2 (2016) 1500409.
[21] Z. Xu, X. Chen, S. Zhang, et al., Phys. Chem. Chem. Phys. 18 (2016) 13209–13215.

[22] W. Tu, Y. Liu, M. Chen, et al., Chin. Chem. Lett. 34 (2023) 107322.
[23] T.Q. Trung, S. Ramasundaram, S.W. Hong, N.E. Lee, Adv. Funct. Mater. 24 (2014) 3438–3445.
[24] T.Q. Trung, N.T. Tien, D. Kim, et al., Adv. Mater. 24 (2012) 5254–5260.
[25] P. Sun, M. Zhu, K. Wang, et al., ACS Appl. Mater. Interfaces 5 (2013) 9563–9571.
[26] M.R. Adib, Y. Lee, V.V. Kondalkar, et al., ACS Sens. 6 (2021) 1012–1021.
[27] W. Xiao, L. Wang, B. Li, et al., J. Colloid Interface Sci. 608 (2022) 931–941.
[28] Y. Zeng, T. Li, Y. Yao, et al., Adv. Funct. Mater. 29 (2019) 1901388.
[29] T. Wang, J. Zhao, C. Weng, et al., J. Mater. Chem. C 9 (2021) 7444–7451.
[30] S. Ryu, L. Liu, S. Berciaud, et al., Nano Lett. 10 (2010) 4944–4951.
[31] Y. Yang, R. Murali, Appl. Phys. Lett. 98 (2011) 093116.
[32] H. Yan, B. Xu, S. Shi, C. Ouyang, J. Appl. Phys. 112 (2012) 104316.
[33] Z. Liu, Z. Zhao, Y. Wang, et al., Adv. Mater. 29 (2017) 1606207.
[34] R. Nair, H. Wu, P.N. Jayaram, et al., Science 335 (2012) 442–444.
[35] S. Lettieri, V. Gargiulo, D.K. Pallotti, et al., Catal. Today 315 (2018) 19–30.
[36] H. Jung, Mater. Lett. 314 (2022) 131758.
[37] A. Ziletti, A. Carvalho, D.K. Campbell, et al., Phys. Rev. Lett. 114 (2015) 046801.
[38] S.M. Sze, K.K. Ng, Physics of Semiconductor Devices, 3th, John Wiley & Sons Inc., New Jersey, 2006.